Research in Astron. Astrophys. **2009** Vol. **9** No. **12**, 1368–1376
*http://www.raa-journal.org* *http://www.iop.org/journals/raa*

***R**esearch in*
***A**stronomy and*
***A**strophysics*

# Two types of dynamic cool coronal structures observed with *STEREO* and *Hinode* *

Jun Zhang and Le-Ping Li

Key Laboratory of Solar Activity, National Astronomical Observatories, Chinese Academy of Sciences, Beijing 100012, China; *zjun@ourstar.bao.ac.cn*

Received 2009 June 2; accepted 2009 September 9

**Abstract** Solar coronal loops show significant plasma motions during their formation and eruption stages. Dynamic cool coronal structures, on the other hand, are often observed to propagate along coronal loops. We report on the discovery of two types of dynamic cool coronal structures, and characterize their fundamental properties. Using the EUV 304 Å images from the Extreme UltraViolet Imager (EUVI) telescope on the Solar TErrestrial RElation Observatory (*STEREO*) and the Ca II filtergrams from the Solar Optical Telescope (SOT) instrument on *Hinode*, we study the evolution of an EUV arch and the kinematics of cool coronal structures. The EUV 304 Å observations show that a missile-like plasmoid moves along an arch-shaped trajectory, with an average velocity of 31 km $s^{-1}$. About three hours later, a plasma arch forms along the trajectory, subsequently the top part of the arch fades away and disappears; meanwhile the plasma belonging to the two legs of the arch flows downward to the arch's feet. During the arch formation and disappearance, SOT Ca II images explore dynamic cool coronal structures beneath the arch. By tracking these structures, we classify them into two types. Type I is thread-like in shape and flows downward with a greater average velocity of 72 km $s^{-1}$; finally it combines with a loop fibril at a chromospheric altitude. Type II is shape-transformable and sometimes rolling as it flows downward with a smaller velocity of 37 km $s^{-1}$, then disappears insularly in the chromosphere. It is suggested that the two types of structures are possibly controlled by different magnetic configurations.

**Key words:** Sun: chromosphere — Sun: UV radiation — Sun: activity

## 1 INTRODUCTION

The solar atmosphere is extremely complex and magnetically structured. Coronal loops, magnetically closed structures in the upper solar atmosphere, exhibit intrinsically dynamic behavior (De Groof et al. 2004, 2005; Doyle et al. 2006; O'Shea et al. 2007a,b), and dynamic coronal structures are often seen to propagate along these loops (Engvold et al. 1979; Loughhead & Bray 1984; Brekke et al. 1997). Material condensing in the corona and appearing to rain down into the chromosphere as observed at the solar limb is termed "coronal rain," originally based on H$\alpha$ observations (Tandberg-Hanssen 1974). Levine & Withroe (1977) presented observations of an active region loop system which underwent a sudden disruption leading to the evacuation of most of the material initially present below a temperature of about $2\times10^6$ K. Kjeldseth-Moe & Brekke (1998) studied the temporal variability of active region loops with the Coronal Diagnostic Spectrometer (CDS), and reported significant changes of coronal

* Supported by the National Natural Science Foundation of China.

loops over a period of one hour, in particular seen in emission lines in the temperature range between $1 \times 10^5 - 5 \times 10^5$ K. This variability is accompanied by large Doppler shifts, typically around $50-100$ km s$^{-1}$. Observations of downflows above large-scale post-flare arcades were first reported by McKenzie & Hudson (1999) using the soft X-ray observations. These downflows are described as dark structures moving through the corona towards the Sun with velocities in the range of $45-500$ km s$^{-1}$. Observations with the Extreme-ultraviolet Imaging Telescope (EIT) with high temporal cadence furthermore reveal spatially localized brightening in coronal loops, moving rapidly down towards the footpoints of the loops (De Groof et al. 2004, 2005). Even under a quiescent condition, with no flares, loops show a strong temporal variability of emission in UV spectral lines and substantial plasma flows. Schrijver (2001) presented a detailed study of the "catastrophic cooling" and evacuation of quiescent coronal loops observed by the Transition Region And Coronal Explorer (*TRACE*), and showed that loop evacuation occurs frequently after plasma in the upper parts of the loops has cooled to the transition region or lower temperatures. The cooling process is often accompanied by emission in C IV (1548 Å) and Ly $\alpha$, developing initially near the top of the loop. Spectroscopic investigations of loops show that the intensity variations have different signatures in UV spectral lines and exhibit Doppler shifts of $20-130$ km s$^{-1}$ (Fredvik et al. 2002).

The physical explanation generally given for dynamic coronal structures is that the plasma which was evaporated into the tops of loops (Forbes & Malherbe 1986; Svestka et al. 1998) radiates away its energy and cools down. The fact that coronal loops undergo rapid evacuation has been known for decades. Thereafter, the cool plasma is observed to slide down on both sides of the loop toward the footpoints with velocities of up to 100 km s$^{-1}$. Shimojo et al. (2002) carried out a set of joint observations with *TRACE* and the Hida/Domeless Solar Telescope (DST) and concluded that the coronal rains over the active region are produced by transient coronal loop brightenings or microflares. Innes et al. (2003a,b) reported similar features detected in EUV by *TRACE* and *SOHO*/Solar Ultraviolet Measurements of Emitted Radiation (SUMER). The downflow here was observed as a dark trail of plasma moving towards the Sun at *TRACE* 195 Å and in the Fe XXI & UV continuum by SUMER. Based on these observations, Innes et al. (2003a,b) concluded that the dark trails of the plasma are likely to be the plasma voids introduced by McKenzie & Hudson (1999). Asai et al. (2004) used the observations of *TRACE* and *RHESSI* to identify a time correlation between non-thermal radiation in the hard X-ray spectra and the times of downflows, and concluded that the downflow motions occurred when large amounts of magnetic energy was released, suggesting a relation of downflows with reconnection outflows. Tripathi et al. (2006) studied a distinct downflow in the course of a prominence eruption associated with a CME, and provided support for the pinching off of the field lines drawn-out by the erupting prominences and the contraction of the arcade formed by the reconnection.

In this paper, for the first time, we report two types of dynamic cool coronal structures which display different behavior in three aspects: falling manners, falling velocities and disappearing patterns, based on high tempo-spatial observations. Other activities, e.g. evolution of plasma clouds, are also described.

## 2 OBSERVATIONS

The Extreme UltraViolet Imager (EUVI) telescope on the Solar TErrestrial RElation Observatory (*STEREO*, Howard et al. 2008) monitors the solar chromosphere and corona. The detectors of EUVI have a field-of-view out to 1.7 $R_\odot$, and observe in four spectral channels that span the 0.1 to 2.0 MK temperature range. The Solar Optical Telescope (SOT) instrument on *Hinode* (Tsuneta et al. 2008), on the other hand, explores a continuous, seeing-free series of diffraction-limited images in a $3880-6680$ Å range with very high tempo-spatial resolutions. On 2007 May 10, there was an arch, which was located on the eastern limb (S02E90) of the Sun, and observed by the EUVI. In this study, we employ the EUV 304 Å (60 000$-$80 000 K) images to investigate the evolution of the arch. The observational mode of the 304 Å images is 1.59″ per CCD pixel with a cadence of 38 s. The Ca II (10 000$-$20 000 K) filtergrams from SOT detected a sub-area underneath the arch. These filtergrams have a spatial resolution of 0.22″, with a cadence of 20 s. Figure 1 displays an EUV 304 Å image from EUVI (left) and a Ca II image from SOT (right).

### 2.1 Dynamics of the Arch

Solar coronal arches (or loops) can be detected when observed in coronal UV and EUV lines (Zhang & Wang 2000, 2001; Anzer et al. 2007). During the formation stage of coronal arches, significant plasma motions are always observed. Similarly, mass motions are also distinct during the disappearance of loops. Figure 2 shows the time sequence of the EUV 304 Å images from EUVI. The top row displays the motion of a missile-like plasmoid (denoted by the arrows). The plasmoid moved along an arch-shaped trajectory. From 17:49 UT to 18:08 UT, when the plasmoid rose to the apex of the arch trajectory, the moving velocities decreased from 35 to 24 km $s^{-1}$. Then the plasmoid fell downward from the apex. The falling velocities increased monotonically, and at 18:46 UT, the velocity reached 36 km $s^{-1}$. To reduce the error in the determination of these velocities, we measure each velocity in a time interval of about 10 min. The uncertainty of the plasmoid position (one pixel, 1.59″) results in a velocity error of 2 km $s^{-1}$. Almost three hours later, the plasma brightened continuously along the former plasmoid trajectory, and the arrows in the bottom row denote the front edge of the brightening plasma. At 22:53 UT, the plasma inside the other leg of the arch also brightened to meet the foregoing plasma, thus making the plasma arch connecting the two legs, with a length of ∼200 Mm. Subsequently, the material in the top part of the arch faded away, the material within the two legs moved downward to the two feet of the arch, then the arch disappeared in 20 min.

### 2.2 Kinematics of Cool Coronal Structures and Plasma Clouds underneath the Arch

From 2007 May 10, 21:20 to 23:59 UT, the target of the SOT Ca II images was the eastern solar limb region located underneath the arch (see Fig. 1). Dynamic structures and plasma clouds were detected during the observations. Figure 3 presents the evolution of two structures from the Ca II filtergrams. The left column displays the falling process of the first structure (see the arrows) which was initially detected at 22:05:00 UT. This structure appeared threadlike (i.e., elongated) in shape, and fell directly downward to the solar chromosphere. In order to compare with the free-fall tracks, we used the height of the falling structures to the solar surface to calculate the falling velocity. Furthermore, all the structures were generally falling vertically with respect to the solar surface. The centers of gravity of the structures are considered as their position. Under this condition, we get a velocity of 75 km $s^{-1}$. At 22:07:19 UT, the structure split into two segments (see the two arrows). The two segments continuously fell downward with a nearly constant velocity. Just before they met two detectable loop fibrils (indicated by two dotted lines at 22:08:42 UT), their velocities decreased from 75 to 60 km $s^{-1}$.

The evolution of the second dynamic structure is shown in the right column of Figure 3. The difference between these two structures is mainly manifested on three aspects. The first one is the falling manner. The shape of this structure changed continuously as it fell downward. Sometimes the shape is threadlike (indicated by dotted lines), and sometimes a drop (see the arrows). It is noticed that the structure rotated about 50° from 22:22:41 to 22:25:41 UT, before the structure split into two parts. The second one is falling velocity. From 22:22:41 to 22:26:21 UT, the velocity of the dynamic structure was 52 km $s^{-1}$ on average, about 20 km $s^{-1}$ lower than the falling velocity of the first structure, then it decreased to 38 km $s^{-1}$. The last aspect is the disappearing patterns. This structure disappeared insularly at a height of 5.5 Mm over the solar surface; no loop was detected beneath the disappearing position of the structure.

Based on their disappearing patterns, we classify these dynamic structures into two types. Type I includes 16 isolated structures which disappear by merging with the loop fibril. These structures are tracked while they fall downward from the corona to the chromosphere. Type II includes 10 isolated structures which disappear insularly in the chromosphere. They are also tracked during their falling downward. Figure 4 displays the relationship between the falling velocities of dynamic structures and the height to the solar surface. The solid circles represent the 16 structures of type I, and the hollow circles, the 10 structures of type II. It indicates that the type I structures fall at greater velocities, with an average value of 72 km $s^{-1}$. However, the type II structures move slowly downward with an average velocity of 37 km $s^{-1}$, which is only half the falling velocity of the type I structures. Comparing the

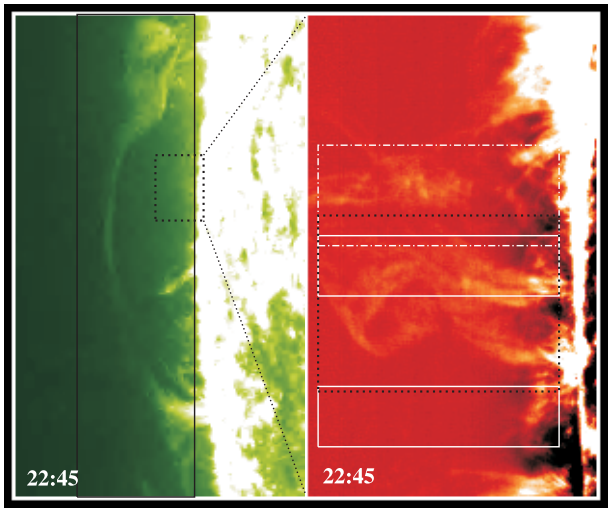


**Fig. 1** An EUV 304 Å image (*left*) from EUVI on *STEREO* and a Ca II image (*right*) from SOT aboard *Hinode* on 2007 May 10. In the EUV 304 Å image, the larger box encloses an arch (see Fig. 2), and the smaller box underneath the arch, outlines the field-of-view (FOV) of the right Ca II filtergram. The two solid rectangular windows in the Ca II image denote sub-areas where individual dynamic structures flow downward from the corona to the chromosphere (see details in Fig. 3), the dash-dotted window, the area where plasma shows waterfall-like motion (see also Fig. 5), and the dotted window, the region in which plasma displays cyclone-like motion (see Fig. 6). The FOV for the EUVI image is about $238'' \times 397''$, and $33'' \times 55''$ for the SOT Ca II filtergram.

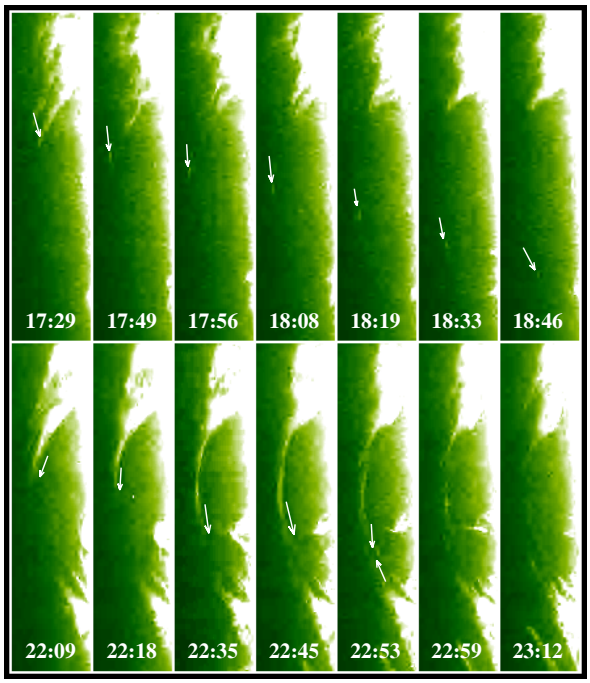


**Fig. 2** Time sequence of the EUV 304 Å images (see the larger rectangular window in the left panel of Fig. 1) showing the dynamics of the arch. The arrows are described in the text. The FOV is about $95'' \times 397''$.

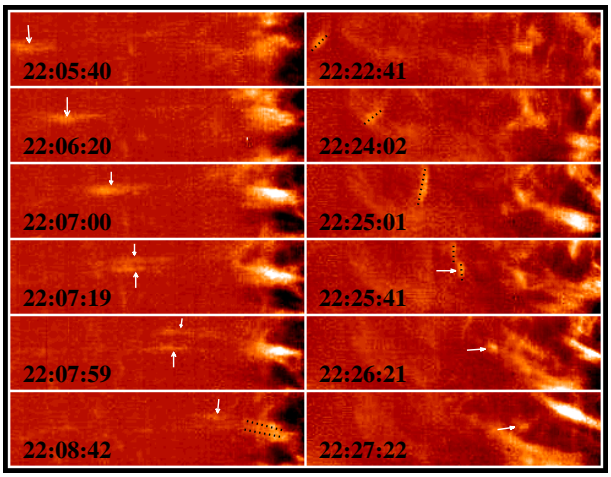


**Fig. 3** Time sequence of the Ca II filtergrams showing the evolution of two dynamic structures. The left column corresponds to the region of the lower solid rectangular window in the right panel of Fig. 1, and the right column to the region of the upper solid rectangular window. The FOV is about $26.4'' \times 6.6''$. The arrows and dotted lines are described in the text.

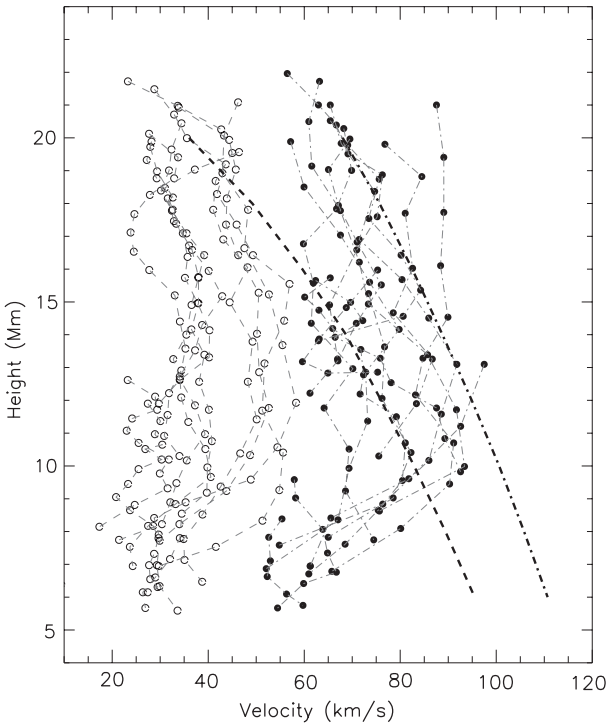


**Fig. 4** Relationship between the downflow velocities of the dynamic structures and the height from the solar surface. The solid circles and the hollow circles denote the velocities of the two types of dynamic structures (see the text), respectively. The individual trajectories (the dash-dotted curves connecting the solid circles, and dashed curves the hollow circles) of the 26 dynamic structures are plotted. The two heavy curves representing the free-fall tracks are fitted to the observed falling velocities at the heights where the bright dynamic structures are detected.

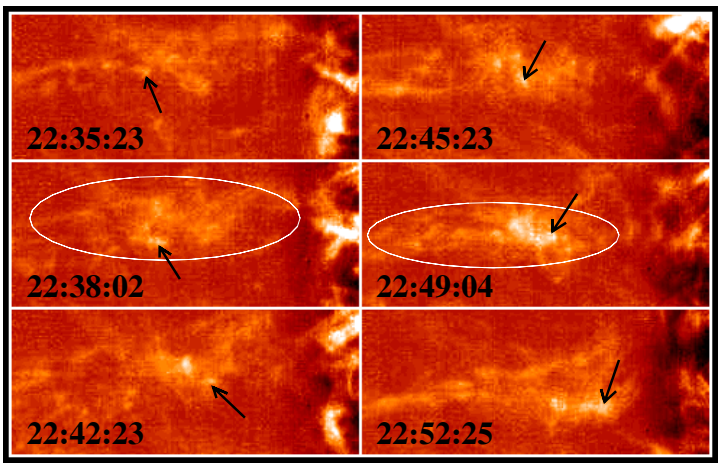


**Fig. 5** Time sequence of the Ca II filtergrams (see the dash-dotted window in the right panel of Fig. 1) showing the evolution of waterfall-like plasma. The FOV is about $26.4'' \times 11''$. The arrows and two ellipses are described in the text.

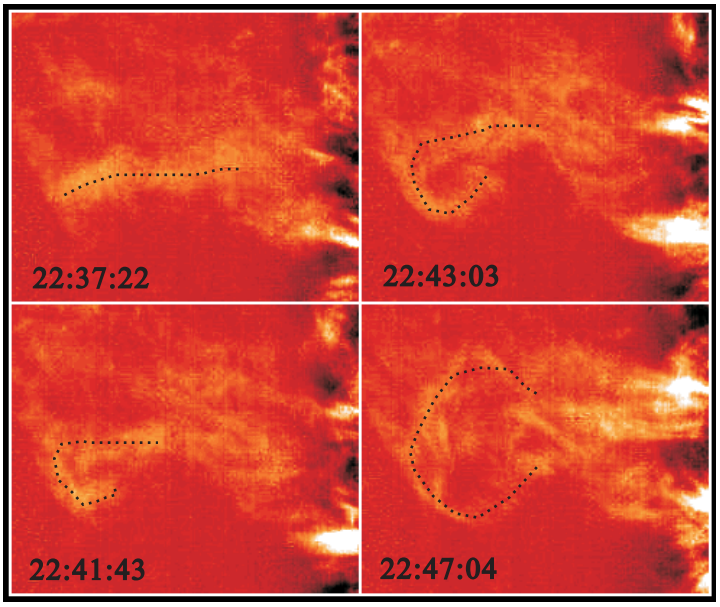


**Fig. 6** Time sequence of the Ca II filtergrams (see the black dotted window in the right panel of Fig. 1) showing the cyclone-like motion of plasma. The FOV is about $26.4'' \times 22''$. The curves are described in the text.

observed falling velocities with calculated free-fall tracks, we find that all the dynamic structures deviate distinctly from the free-fall tracks, while they are close to the solar limb.

The measured falling velocities of these dynamic structures only represent the projective component of true velocities; they are affected by the angle between the moving direction of these structures and the line-of-sight of the observer. De Groof et al. (2004) have discussed the projection effect. Theoretically,

the projection effect (see fig. 10 of De Groof et al. 2004) cannot cause obvious speed deviation, while all the dynamic structures are close to the limb. The main error source of velocity determination is due to uncertainty in the dynamic structure position. A position error of one pixel introduces an error in the velocity of (one pixel)/(time interval). As the size of one pixel is about $0.11''$ and the time interval is about 20 s, the error in velocity becomes 4 km $s^{-1}$, which may explain a part of the scatter in Figure 4. However, it is clear that the velocity error is much smaller than the falling velocity difference (35 km $s^{-1}$) of the two types of dynamic structures. This implies that the velocity difference actually exists.

Besides the individual dynamic structures, there are other kinds of plasma structures. Figure 5 shows the evolution of cloud-built plasma. The plasma within each ellipse region falls as a whole downward to the chromosphere, but the velocities are not unique. There are some bright structures (see the arrows), which become larger and larger in size during their falling downward. The average velocity of these structures is about 11 km $s^{-1}$. In the observational interval, there are two such cases. Considering the sizes of these structures, we speculate that they may correspond with coronal rains reported before (Zirin 1974). Some plasma clouds, however, do not fall downward. Figure 6 shows a cyclone-like motion of a plasma cloud. The dotted curves represent the central axes of the cloud at different evolution stages. At 22:37:22 UT, the axis was nearly vertical to the solar surface, then the axis bent at the top part to form a fishhook-shaped structure. This structure became larger and larger in size, then diffused and disappeared in half an hour.

## 3 CONCLUSIONS AND DISCUSSION

We first report on the observations of two types of dynamic structures underneath an arch. Type I structures fall downward with greater velocities, and disappear by combining detectable loop fibrils. However, type II ones fall with smaller velocities, then disappear insularly in the chromosphere. It has been identified that all the dynamic structures deviated remarkably from free-fall tracks, while they are close to the solar limb. In addition, other kinds of plasma structures, e.g. cloud-built plasma, also exist in the corona and upper chromosphere. These plasma clouds either move downward to the lower chromosphere, or display cyclone-like motion.

The difference in the falling velocities between these two types of structures may be affected by the magnetic configuration, as showed in Figure 7. From this figure, we can see that type I structures fall along slick magnetic loops which are mainly perpendicular to the solar surface. For type II structures, however, a more complicated magnetic configuration may respond to their strange kinematics, i.e. undergoing rotation and falling along tortuous paths instead of going straight down. For a better comparison with the observations displayed in Figure 3, we show the actual observation times (shown in Fig. 3) in Figure 7. Malville (1976) has also suggested that material falling in distorted flux ropes experiences a Lorentz force, thus making the structures fall slower.

The departures of the dynamic structures from free-fall at lower heights was interpreted in terms of plasma deceleration (Wiik et al. 1996). Heinzel et al. (1992) have suggested three possible explanations for the observed deceleration: variation of the loop magnetic structure during the typical fall-time of the dynamic structures; helicity of the magnetic field inside the loop; and deceleration of the cool structures as they move inside a hotter plasma. In this work, whether the first explanation is appropriate for the departure is still in question, as the variation of loops cannot be reliably detected in our observations. The last explanation can be considered at lower heights where cool structures compress a hot plasma as in a piston. Using MHD simulations, Mackay & Galsgaard (2001) have considered falling high density material in a stratified atmosphere, and they produced a piston type model to interpret the deceleration of plasma. For the fast falling dynamic structures, the piston mechanism may play a key role, as the bright (hot and/or denser) plasma at the footpoints of the fibrils is detected (see Fig. 3). For the slow falling ones, the second explanation is possible, as there exists some evidence that these structures move along twisted magnetic loops. Mein et al. (1996) observed similar departures from free-fall in the case of downflows in arch filament systems, and proposed another good candidate for deceleration. They

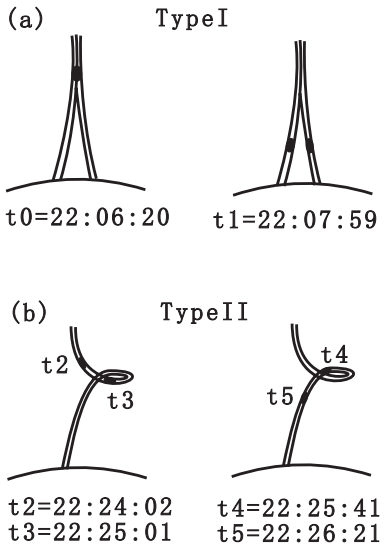


**Fig. 7** Schematic diagrams illustrating the evolution of the type I dynamic coronal structures at t0 and t1 (a), and type II dynamic coronal structures at t2, t3, t4, and t5 (b), respectively. t0, t1, t2, t3, t4, and t5 are the observation times displayed in Fig. 3. The solid lines represent the magnetic field lines, as well as the solid points, the dynamic coronal structures.

suggested that a deceleration may result from shock waves generated at the footpoints, presumably due to the interaction of downflows with denser parts of the atmosphere.

The formation of these dynamic structures is also an intriguing problem. Generally, dynamic cool coronal structures are the result of the cooling of the hot coronal loops which we typically observe at somewhat higher altitudes. Shimojo et al. (2002) once concluded that the coronal rains over the active region are produced by transient coronal loop brightenings or microflares. Müller et al. (2003, 2005) presented a comparison of observed intensity enhancements from an EIT shutterless campaign with non-equilibrium ionization simulations of coronal loops in order to reveal the physical processes governing fast flows and localized brightenings. They show that catastrophic cooling around the loop apex as a consequence of footpoint-concentrated heating can perhaps offer a simple explanation for these observations. In this paper, the cool dynamic structures also appeared under a dynamic EUV arch, which may be related with the formation and disappearance of the arch. Further study of dynamic structures will require new optical and UV spectral observations with high resolution. This would allow us to possibly make a reliable geometrical reconstruction of the true loop shapes, and to derive the plasma parameters more accurately.

**Acknowledgements** The authors are indebted to the *STEREO* and *Hinode* teams for providing the data. *Hinode* is a Japanese mission developed and launched by ISAS/JAXA, with NAOJ as a domestic partner and NASA and STFC (UK) as international partners. It is operated by these agencies in co-operation with ESA and NSC (Norway). This work is supported by the National Natural Science Foundation of China (Grant Nos. 40890161 and 40674081), the CAS Project KJCX2-YW-T04, and the National Basic Research Program of China (Grant No. G2006CB806303).

## References

Anzer, U., Heinzel, P., & Fárnik, F. 2007, Solar Phys., 242, 43
Asai, A., Yokoyama, T., Shimojo, M., & Shibata, K. 2004, ApJ, 605, L77
Brekke, P., Kjeldseth-Moe, O., & Harrison, R. A. 1997, Solar Phys., 175, 511
De Groof, A., Berghmans, D., van Driel-Gesztelyi, L., & Poedts, S. 2004, A&A, 415, 1141
De Groof, A., Bastiaensen, C., Müller, D. A. N., Berghmans, D., & Poedts, S. 2005, A&A, 443, 319
Doyle, J. G., Taroyan, Y., Ishak, B., Madjarska, M. S., & Bradshaw, S. J. 2006, A&A, 452, 1075
Engvold, O., Jensen, E., & Andersen, B. N. 1979, Solar Phys., 62, 331
Forbes, T. G., & Malherbe, J. M. 1986, ApJ, 302, L67
Fredvik, T., et al. 2002, Adv. Space Res., 30, 635
Heinzel, P., Schmieder, B., & Mein, P. 1992, Solar Phys., 139, 81
Howard, R. A., et al. 2008, Space Sci. Rev., 136, 67
Innes, D. E., McKenzie, D. E., & Wang, T. 2003a, Solar Phys., 217, 247
Innes, D. E., McKenzie, D. E., & Wang, T. 2003b, Solar Phys., 217, 267
Kjeldseth-Moe, O., & Brekke, P. 1998, Solar Phys., 182, 73
Levine, R. H., & Withbroe, G. L. 1977, Solar Phys., 51, 83
Loughhead, R. E., & Bray, R. J. 1984, ApJ, 283, 392
Mackay, D. H., & Galsgaard, K. 2001, Solar Phys., 198, 289
Malville, J. M. 1976, Solar Phys., 50, 79
Mckenzie, D. E., & Hudson, H. S. 1999, ApJ, 519, 93
Mein, P., et al. 1996, A&A, 305, 343
Müller, D. A. N., Hansteen, V. H., & Peter, H. 2003, A&A, 411, 605
Müller, D. A. N., De Groof, A., Hansteen, V. H., & Peter, H. 2005, A&A, 436, 1067
O'Shea, E., Srivastava, A., Doyle, J., & Banerjee, D. 2007a, A&A, 473, L13
O'Shea, E., Banerjee, D., & Doyle, J. G. 2007b, A&A, 475, L25
Schrijver, C. J. 2001, Solar Phys., 198, 325
Shimojo, M., Kurokawa, H., & Yoshimura, K. 2002, Solar Phys., 206, 133
Svestka, Z. K., Fárník, F., Hudson, H. S., & Hick, P. 1998, Solar Phys., 182, 179
Tandberg-Hanssen, E. 1974, Solar Prominences, 12 (Dordrecht-Holland/Boston-USA: D. Reidel Publishing Company), 29
Tripathi, D., Solanki, S. K., Schwenn, R., et al. 2006, A&A, 449, 369
Tsuneta, S., et al. 2008, Solar Phys., 249, 167
Wiik, J. E., Schmieder, B., Heinzel, P., & Roudier, T. 1996, Solar Phys., 166, 89
Zhang, J., & Wang, J. 2000, Geophys. Res. Lett., 27, 2877
Zhang, J., & Wang, J. 2001, ApJ, 554, 474
Zirin, H. 1974, Solar Phys., 38, 91